Research Article | Vol. 27, No. 25 / 9 December 2019 / Optics Express 36580
Optics EXPRESS

Light-sheet imaging for the recording of transverse absolute density distributions of gas-phase particle-beams from nanoparticle injectors

LENA WORBS,[1,2] JANNIK LÜBKE,[1,2,3] NILS ROTH,[1,2] AMIT K. SAMANTA,[1] DANIEL A. HORKE,[1,3,4] AND JOCHEN KÜPPER[1,2,3,*]

[1]Center for Free-Electron Laser Science, Deutsches Elektronen-Synchrotron DESY, Notkestrasse 85, 22607 Hamburg, Germany
[2]Department of Physics, Universität Hamburg, Luruper Chaussee 149, 22761 Hamburg, Germany
[3]Center for Ultrafast Imaging, Universität Hamburg, Luruper Chaussee 149, 22761 Hamburg, Germany
[4]Institute for Molecules and Materials, Radboud Universiteit, Houtlaan 4, 6525 XZ Nijmegen, The Netherlands
*jochen.kuepper@cfel.de

Abstract: Imaging biological molecules in the gas-phase requires novel sample delivery methods, which generally have to be characterized and optimized to produce high-density particle beams. A non-destructive characterization method of the transverse particle beam profile is presented. It enables the characterization of the particle beam in parallel to the collection of, for instance, x-ray-diffraction patterns. As a rather simple experimental method, it requires the generation of a small laser-light sheet using a cylindrical telescope and a microscope. The working principle of this technique was demonstrated for the characterization of the fluid-dynamic-focusing behavior of 220 nm polystyrene beads as prototypical nanoparticles. The particle flux was determined and the velocity distribution was calibrated using Mie-scattering calculations.

1. Introduction

Knowledge of the structure of biological molecules, such as proteins or viruses, is fundamental for understanding their function. A recently pioneered approach for directly recording high-resolution structures of intact single molecules is single-particle coherent diffractive imaging using x-ray free-electrons lasers (XFELs) [1,2]. To reconstruct a three-dimensional molecular structure, this approach requires the collection of a large number of individual diffraction patterns from single molecules [3,4]. In order to achieve this within the limited amount of time available at central XFEL facilities, therefore, requires a high particle flux in the gas-phase. Furthermore, as the samples investigated get smaller in size, now approaching the limit of single proteins, the necessary x-ray intensity for recording a single-shot diffraction pattern increases. Experimentally, this higher intensity is typically achieved by focusing the x-ray beam to a smaller spot, in SPI experiments typically to sizes of only ~ 100 nm. This places stringent demands on the employed sample delivery methods, typically aerodynamic lens stacks (ALS) [5–7], and requires their characterization and optimization prior to XFEL experiments with laboratory-based methods.

Any characterization method for nanoparticle injectors would ideally reconstruct the full six-dimensional phase space of nanoparticles emitted, and would do so on-the-fly, *in situ*, non-destructive, and universally for any nanoparticle. Furthermore, the simultaneous characterization of sheath gas flows would be advantageous, but that seems to be well delegated to offline analysis [8]. None of the currently available nanoparticle-imaging methods fulfills all these requirements [9]. The most commonly employed method is optical imaging of the particle stream using side-illumination with a laser beam [9]. This allows one to measure the longitudinal position

#378458 https://doi.org/10.1364/OE.27.036580
Journal © 2019 Received 27 Sep 2019; revised 15 Nov 2019; accepted 15 Nov 2019; published 2 Dec 2019

Optics EXPRESS

of nanoparticles, as well as their longitudinal velocity through the use of double-pulse lasers [10], commonly termed *particle imaging velocimetry*, or by recording light streaks from the particles through the use of appropriate illumination or exposure times [9]. While this side-view light-scattering approach fulfills the requirements for *in situ* operation and largely the universality for any nanoparticle, it does not detect asymmetries in the transverse nanoparticle beam profile without scanning the laser focus through the particle beam. For larger particle beams this approach can, furthermore, suffer from a mismatch between particle beam size and focal depth of the used imaging objective.

A direct way to record the transverse profile of particles has so far only been available through so-called dusting, where particles are caught on a sticky surface in-vacuum, which is subsequently imaged [9]. This approach has the obvious drawback of being destructive. Furthermore, it does not allow the recording of absolute particle densities, as the sticking probability of particles is not unity, nor of particle velocities.

Here, we present a different approach, combining the advantages of laser-based scattering microscopy with the ability to measure transverse particle positions: light-sheet imaging (LSI). A sheet of light is generated and the scattered light from the particles passing through the sheet is collected using a microscope. This method provides a simple, non-destructive, and *in situ* method to record transverse particle beam profiles, including absolute number densities, as well as the velocity of particles passing through the light sheet. For best general applicability and overall characterization of the injection we employed a continuous detection scheme, which provides the maximal information on the sample beam and enables the characterization for any x-ray repetition rate. However, the method is general and could as well be utilized with a pulsed-laser illumination, e. g., a synchronized optical laser provided by the x-ray facility [11].

2. Experimental setup

A schematic overview of the LSI setup is shown in Fig. 1. It mainly consisted of three parts: the optical setup for the generation of the light sheet from a continuous-wave laser, an ALS to generate a nanoparticle beam, and a microscope-detector setup for recording the scattered light.

The light sheet was generated from a continuous-wave laser system (Coherent Verdi V, 5 W, 532 nm), operated at 0.5 W and with vertical polarization. The initial beam diameter of 2.25(23) mm is increased by a factor of two using a Galilean telescope ($f_{L1} = -50$ mm, $f_{L2} = 100$ mm); throughout the manuscript all laser-beam widths are specified to the $1/e^2$ intensity. A second cylindrical-lens telescope ($f_{L3} = -50$ mm, $f_{L4} = 150$ mm) further increases the vertical diameter of the beam by a factor of three, yielding an elliptical beam with a vertical width of $h = 13.5$ mm and a horizontal width of $w = 4.1$ mm. This beam is focused using a cylindrical lens ($f_{L5} = 300$ mm), generating the light sheet in the center of the vacuum chamber. The created light sheet has a thickness of 24.8 µm (14.6 µm full-width-half-maximum, FWHM), a Rayleigh length of $z_R = 1.5$ mm, and a horizontal width of $w = 4.1$ mm. The corresponding maximum power density in the focus is $\sim 2.8 \times 10^3$ W/cm^2, well below the typical damage threshold for nanoparticles.

The nanoparticle beam was generated using a previously described ALS [7]. Briefly, 220 nm polystyrene beads in solution (Alfa Aesar, particle size 220 ± 17.3 nm) were diluted to 5×10^6 particles/ml and aerosolized using a gas-dynamic virtual nozzle (GDVN) [12,13]. Following a differential pumping stage, nanoparticles entered the ALS, which produced a tightly collimated and focused particle stream in the vacuum chamber; the chamber pressure was typically held at 6×10^{-5} mbar during experiments. The entire ALS system was placed on a motorized *xyz*-translation stage to allow accurate positioning of the particle stream.

Particles emerging from the the ALS passed through the light sheet and the scattered light was collected by a camera-based microscope system. This consisted of a long working-distance objective (Edmund Optics, 5× magnification, numerical aperture 0.14, working distance 34 mm) with a depth of view of 14 µm, chosen to match the sheet thickness to get sharp images of particle

Optics EXPRESS

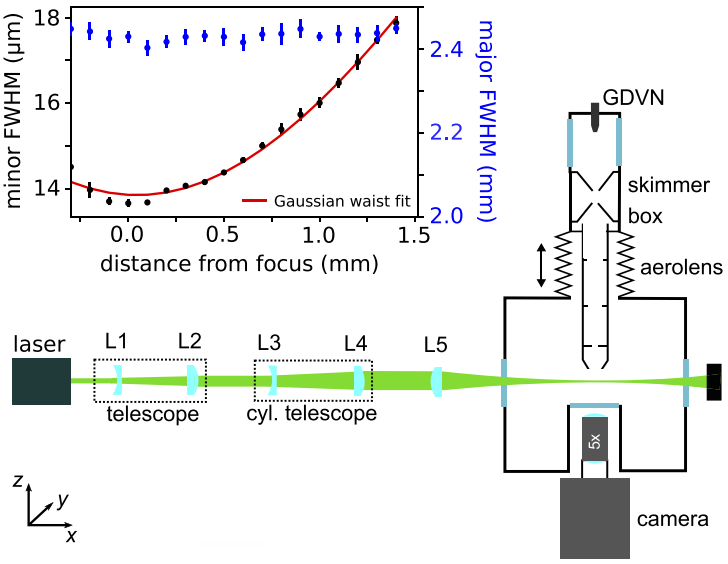

Fig. 1. Schematic of the light-sheet imaging setup for the characterization of nanoparticle beams emerging from an aerodynamic lens stack. The light sheet is generated using a spherical telescope, a cylindrical-lens telescope, and a spherical focusing lens to create an elliptical focus. The inset shows the measured values of the minor, z, and major, y, widths along the light beam and the corresponding Gaussian beam-waist fit to determine the Rayleigh length $z_R = 1.5$ mm. Light is detected with a microscope and camera setup along the y direction.

scatter, and a high-efficiency sCMOS camera (Photometrics Prime 95B, quantum efficiency 0.95 at 532 nm, 1200 × 1200 pixels). This yields a nominal resolution of 0.54 px/µm. Images were collected with a 1 ms exposure time and at a frame rate of 82 fps at full-frame size. Collected images were analyzed using a centroiding algorithm based on Hessian blob-finding [14], yielding sub-pixel particle positions as well as an accurate estimate of the number of recorded photons per particle.

The data shown were typically recorded for 2 000 frames and limited to a region of interest covering 350 × 350 pixels. Transverse beam profiles were generated as 2D histograms of the recorded particle positions. For the full three-dimensional reconstruction of the particle beam, the distance between the ALS exit and the light sheet was varied to build up a series of 2D transverse profiles. To recover the velocity of particles passing through the sheet, the recorded scattering intensity was compared with calculations based on Mie theory, performed using a homebuilt Python script based on the freely available Bohren and Huffman code [15], taking into account the experimental parameters, e. g., the scattering angle, the numerical aperture, and the particle size.

3. Results and discussion

An example image showing two nanoparticles passing through the light sheet simultaneously is shown in Fig. 2a. Here, the concentration of the nanoparticle solution was reduced from stock to ensure that camera frames contained no more than 2 particles. An example of a measured full particle beam profile is shown in Fig. 2b, recorded 6 mm below the ALS injector. In Fig. 2c, the 3D beam profile is shown as individual 2D histograms recorded at several distances. These measurements directly reveal, for instance, any astigmatism that might be present in the particle beam. From Fig. 2c it is clear that moving away from the injector tip the particle-beam widths

Optics EXPRESS

changes, showing the characteristic focusing behavior of the injector [7]. Recorded particle beam profiles typically show a Gaussian intensity distribution and the evolution of the particle beam can be accurately described by fitting a 2D Gaussian function to the recorded data, thus allowing for an easy evaluation of the beam widths and asymmetry through the minor and major axis of the fitted 2D Gaussian. The analysis of the size at 7 mm downstream the injector reveals that, without any specific optimization of the ALS, we generated a particle beam with a focus FWHM of 44.6(33) µm.

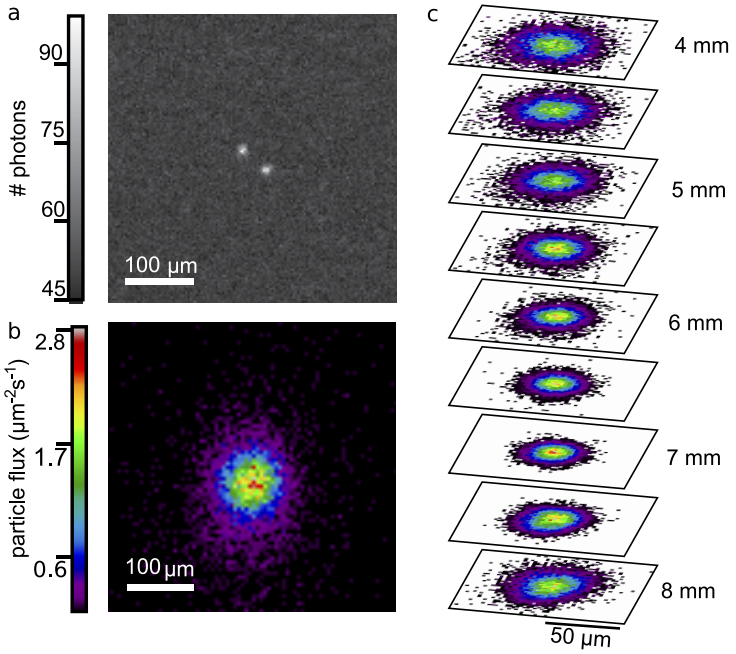

Fig. 2. (a) Raw image of a single camera frame containing two particles. (b) Transverse beam profile 6 mm below the injector tip, shown as a 2D histogram of the determined particle positions; the colorscale represents particle flux. (c) 3D beam profile shown as individual 2D histograms measured at different distances from the ALS exit. The colorscale is the same as in (b).

Since the measurement is based on counting individual particles, the histograms reveal the absolute particle flux, that is, the number of particles per area per second. The rate of particles is recovered from the observation time, which due to the continuous illumination is simply given by the number of frames multiplied by their exposure times. The particle flux can then be calculated from the number of particles detected per pixel or histogram bin. The peak particle flux per µm^2 per second as a function of the distance from the ALS exit is shown in Fig. 3a. Under the given conditions, the maximum particle flux of 4.3 particles/µm^2/s is measured 7.0 mm below the injector tip.

In order to recover the velocity of particles passing through the light sheet, the recorded intensity distribution from single particles was modeled by Mie theory. As the illumination region of the particles is constant, i. e., the thickness of the light sheet, the number of scattered photons depends on the time the particles need to pass the light sheet, i. e., their velocity. From this and the scattering probability as a function of particle size, from Mie theory, we can correlate the number of photons, i. e., the scattered light intensity, recorded per particle with its velocity. We assumed a particle size-distribution of 220 ± 17 nm as specified by the manufacturers. This results in a velocity probability distribution for every single measured particle. The velocity

Optics EXPRESS

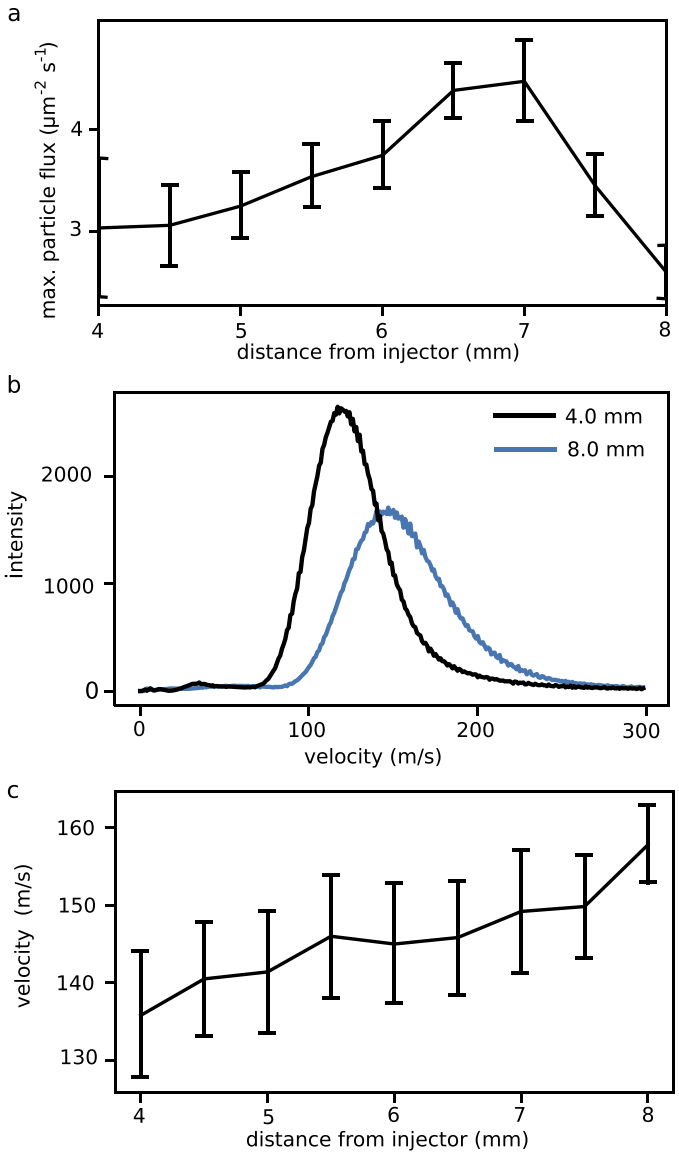

Fig. 3. (a) Maximum particle flux as a function of the distance from the ALS, vertical bars represent the standard errors. (b) Velocity distributions measured at distances of 4 mm (black) and 8 mm (blue) from the ALS. (c) Mean of the velocity distribution depending on the distance from the injector.

distribution of all particles measured at a certain distance from the ALS exit is the sum of the individual velocity probability distributions, see Fig. 3b. At 4 mm (black curve) downstream the ALS exit, the velocity distribution is centered around 122 m/s and the FWHM is 49 m/s. At 8 mm (blue curve) the mean velocity is 151 m/s with a FWHM of 66 m/s. Fig. 3c shows the mean velocity of the particle stream as a function of distance to the ALS exit. Both, mean velocity and the width of the velocity distribution increased with distance from the ALS exit, consistent with recent observations [10]. We ascribe the increasing velocity to acceleration by the helium gas co-emerging from the ALS, hinting at the need to correlate this acceleration with

Optics EXPRESS

measurements of the gas density [8] in future work. The observed velocities above 100 m/s show that the particles are fast enough to clear the interaction region with an x-ray beam in a typical single-particle imaging experiment in between two pulses, assuming a µm beam size, including tails, and the 4.4 MHz repetition rate of the EuXFEL [16].

4. Conclusion

Light-sheet imaging (LSI) provides a non-destructive measurement technique for transverse nanoparticle beam profiles. It is general and applicable to beams from any gas-phase nanoparticle-beam injector. Here, we characterized a nanoparticle beam generated from an aerodynamic lens stack. A light sheet with a thickness comparable to the depth of view of the used microscope objective was generated using cylindrical lenses. The scattered light from the nanoparticles was collected and utilized to determine the particle positions in order to measure the transverse beam profile and the absolute particle flux. The number of collected scattered photons was used for determining the velocity of the nanoparticles.

In current single-particle diffractive-imaging experiments, the initial particle concentration in solution is in the order of 10^{14} particles/ml, which increases the maximum particle flux in our experiment to $\sim 10^7$ particles/µm^2/s, corresponding to $\sim 10^4$ particles/µm^2/frame at 1 ms exposure time. In this case, an *in situ* characterization would be enabled through limited effective illumination, e. g., using a pulsed illumination scheme.

Future single-particle diffractive-imaging experiments on biological molecules, with particle sizes of $\sim$ 10 nm, require the benchmarking of ALSs for such small particle sizes. The use of light-sheet imaging for such small particles requires increased laser powers. In our specific setup, e. g., with a 5 W green laser, the detection of particles is limited to particles down to $\sim$ 100 nm to be distinguishable from noise. The detection of smaller particles, e. g., 10 nm proteins with typical velocities from an ALS of $\sim$ 100 m/s, a cw laser power of 54 MW would be necessary, which is practically infeasible [17]. However, the sizes of these small particles sizes are typically more precisely known *a priori* and pulsed illumination, enabling such strong peak intensities, mimicking or even sub-sampling the XFEL temporal pulse profiles would provide equivalent information. This could still be feasible with standard laser technology routinely available at XFEL facilities.

Funding

Deutsche Forschungsgemeinschaft; Helmholtz Gemeinschaft Deutscher Forschungszentren (Impuls- und Vernetzungsfond).

Disclosures

The authors declare no conflicts of interest.

References

1. R. Neutze, R. Wouts, D. van der Spoel, E. Weckert, and J. Hajdu, "Potential for biomolecular imaging with femtosecond x-ray pulses," Nature **406**(6797), 752–757 (2000).
2. A. Barty, J. Küpper, and H. N. Chapman, "Molecular imaging using x-ray free-electron lasers," Annu. Rev. Phys. Chem. **64**(1), 415–435 (2013).
3. M. J. Bogan, S. Boutet, H. N. Chapman, S. Marchesini, A. Barty, W. H. Benner, U. Rohner, M. Frank, S. P. Hau-Riege, S. Bajt, B. Woods, M. M. Seibert, B. Iwan, N. Timneanu, J. Hajdu, and J. Schulz, "Aerosol imaging with a soft x-ray free electron laser," Aerosol Sci. Technol. **44**(3), i–vi (2010).
4. T. Ekeberg, M. Svenda, C. Abergel, F. R. N. C. Maia, V. Seltzer, J.-M. Claverie, M. Hantke, O. Jönsson, C. Nettelblad, G. van der Schot, M. Liang, D. P. Deponte, A. Barty, M. M. Seibert, B. Iwan, I. Andersson, N. D. Loh, A. V. Martin, H. Chapman, C. Bostedt, J. D. Bozek, K. R. Ferguson, J. Krzywinski, S. W. Epp, D. Rolles, A. Rudenko, R. Hartmann, N. Kimmel, and J. Hajdu, "Three-dimensional reconstruction of the giant mimivirus particle with an x-ray free-electron laser," Phys. Rev. Lett. **114**(9), 098102 (2015).

Optics EXPRESS

5. P. Liu, P. J. Ziemann, D. B. Kittelson, and P. H. McMurry, "Generating particle beams of controlled dimensions and divergence: I. theory of particle motion in aerodynamic lenses and nozzle expansions," Aerosol Sci. Technol. **22**(3), 293–313 (1995).
6. M. F. Hantke, D. Hasse, F. R. N. C. Maia, T. Ekeberg, K. John, M. Svenda, N. D. Loh, A. V. Martin, N. Timneanu, L. S. D van der SchotGijs, G. H. Carlsson, M. Ingelman, J. Andreasson, D. Westphal, M. Liang, F. Stellato, D. P. DePonte, R. Hartmann, N. Kimmel, R. A. Kirian, M. M. Seibert, K. Mühlig, S. Schorb, K. Ferguson, C. Bostedt, S. Carron, J. D. Bozek, D. Rolles, A. Rudenko, S. Epp, H. N. Chapman, A. Barty, J. Hajdu, and I. Andersson, "High-throughput imaging of heterogeneous cell organelles with an x-ray laser," Nat. Photonics **8**(12), 943–949 (2014).
7. N. Roth, S. Awel, D. A. Horke, and J. Küpper, "Optimizing aerodynamic lenses for single-particle imaging," J. Aerosol Sci. **124**, 17–29 (2018).
8. D. A. Horke, N. Roth, L. Worbs, and J. Küpper, "Characterizing gas flow from aerosol particle injectors," J. Appl. Phys. **121**(12), 123106 (2017).
9. S. Awel, R. A. Kirian, N. Eckerskorn, M. Wiedorn, D. A. Horke, A. V. Rode, J. Küpper, and H. N. Chapman, "Visualizing aerosol-particle injection for diffractive-imaging experiments," Opt. Express **24**(6), 6507–6521 (2016).
10. M. F. Hantke, J. Bielecki, O. Kulyk, D. Westphal, D. S. D. Larsson, M. Svenda, H. K. N. Reddy, R. A. Kirian, J. Andreasson, J. Hajdu, and F. R. N. C. Maia, "Rayleigh-scattering microscopy for tracking and sizing nanoparticles in focused aerosol beams," IUCrJ **5**(6), 673–680 (2018).
11. T. Kierspel, J. Wiese, T. Mullins, J. Robinson, A. Aquila, A. Barty, R. Bean, R. Boll, S. Boutet, P. Bucksbaum, H. N. Chapman, L. Christensen, A. Fry, M. Hunter, J. E. Koglin, M. Liang, V. Mariani, A. Morgan, A. Natan, V. Petrovic, D. Rolles, A. Rudenko, K. Schnorr, H. Stapelfeldt, S. Stern, J. Thøgersen, C. H. Yoon, F. Wang, S. Trippel, and J. Küpper, "Strongly aligned molecules at free-electron lasers," J. Phys. B **48**(20), 204002 (2015).
12. D. P. DePonte, U. Weierstall, K. Schmidt, J. Warner, D. Starodub, J. C. H. Spence, and R. B. Doak, "Gas dynamic virtual nozzle for generation of microscopic droplet streams," J. Phys. D: Appl. Phys. **41**(19), 195505 (2008).
13. K. R. Beyerlein, L. Adriano, M. Heymann, R. Kirian, J. Knoska, F. Wilde, H. N. Chapman, and S. Bajt, "Ceramic micro-injection molded nozzles for serial femtosecond crystallography sample delivery," Rev. Sci. Instrum. **86**(12), 125104 (2015).
14. B. P. Marsh, N. Chada, R. R. Sanganna Gari, K. P. Sigdel, and G. M. King, "The Hessian blob algorithm: Precise particle detection in atomic force microscopy imagery," Sci. Rep. **8**(1), 978 (2018).
15. C. F. Bohren and D. R. Huffman, *Absorption and Scattering of Light by Small Particles* (John Wiley & Sons, 1998).
16. R. J. Bean, A. Aquila, L. Samoylova, and A. P. Mancuso, "Design of the mirror optical systems for coherent diffractive imaging at the SPB/SFX instrument of the European XFEL," J. Opt. **18**(7), 074011 (2016).
17. B. Deppe, G. Huber, C. Kränkel, and J. Küpper, "High-intracavity-power thin-disk laser for alignment of molecules," Opt. Express **23**(22), 28491 (2015).